# Study of polycrystalline $Cu_2ZnSnS_4$ films by Raman scattering

P. A. Fernandes[a,b,*], P.M.P. Salomé[a,**], A.F. da Cunha[a]

[a] *I3N- Departamento de Física, Universidade de Aveiro, Campus Universitário de Santiago, 3810-193 Aveiro, Portugal*
[b] *Departamento de Física, Instituto Superior de Engenharia do Porto, Instituto Politécnico do Porto, Rua Dr. António Bernardino de Almeida, 431, 4200-072 Porto, Portugal*

**Abstract**

$Cu_2ZnSnS_4$ (CZTS) is a p-type semiconductor that has been seen as a possible low-cost replacement for $Cu(In,Ga)Se_2$ in thin film solar cells. So far compound has presented difficulties in its growth, mainly, because of the formation of unwanted phases like ZnS, $Cu_xSnS_{x+1}$, $Sn_xS_y$, $Cu_{2-x}S$ and $MoS_2$. X-ray diffraction analysis (XRD), which is mostly used for phase identification cannot resolve some of these phases from the kesterite/stannite CZTS and thus the use of a complementary technique is needed. Raman scattering analysis can help distinguishing these phases not only laterally but also in depth. Knowing the absorption coefficient and using different excitation wavelengths in Raman scattering analysis, one is capable of profiling the different phases present in multi-phase CZTS thin films.

This work describes in a concise form the methods used to grow chalcogenide compounds, such as, CZTS, $Cu_xSnS_{x+1}$, $Sn_xS_y$ and cubic ZnS based on the sulphurization of stacked metallic precursors. The results of the films' characterization by XRD, electron backscattered diffraction and scanning electron microscopy/energy dispersive spectroscopy techniques are presented for the CZTS phase. The limitation of XRD to identify some of the possible phases that can remain after the sulphurization process are investigated. The results of the Raman analysis of the phases formed in this growth method and the advantage of using this technique in identifying them are presented. Using different excitation wavelengths it is also analysed the CZTS film in depth showing that this technique can be used as non destructive methods to detect unwanted phases.

*Keywords:* $Cu_2ZnSnS_4$, thin film, Raman, XRD, EBSD.

## 1. Introduction

$Cu_2ZnSnS_4$ (CZTS) with the kesterite/stannite structure is a p-type semiconductor with an absorption coefficient higher than $10^{-4}$ $cm^{-1}$ and a band gap energy close to 1.5 eV [1, 2]. Because of these characteristics and the fact that it uses no expensive or toxic elements like In, Ga or Se it is seen as a future replacement for $Cu(In,Ga)Se_2$ (CIGS) in thin film solar cells. However, CIGS laboratory solar cells achieved efficiencies up to 20.3 % [3], while for CZTS solar cells the maximum reported efficiency is 6.8% [4]. Before exploring the reasons for this difference, first it is necessary to understand the problem of phase identification in CZTS. X-ray diffraction (XRD) has been widely used as the main tool to analyse the structure of CZTS thin films. In this paper, we are going to show that XRD alone is not sufficient to resolve the different phases that may be present and that Raman scattering is a useful complementary technique not only to identify unwanted phases but also to localize them spatially.

The Raman scattering technique was already used for the study of chalcopyrite compounds such as $CuInS_2$ [5]. The in depth study of the absorber layer of solar cells using Raman scattering has been tested using three different approaches:

1. Takei *et al.* [6] performed a cross sectional scanning of the absorber layer and studied the spectra;
2. Calvo-Barrio *et al.* [7] changed the depth of analysis focusing the measurement point deeper in the absorber layer;
3. the most common approach applies successively sputtering runs to expose the surface of the deeper layers and analyses each exposed surfaces. Álvarez-García *et al.* [8] used this methods combined with Auger electron spectroscopy to study the quality of $CuInS_2$ polycrystalline films.

The need of cutting the samples to look at the cross section and the use of sputtering to erode the surface make both techniques destructive. The main disadvantage of the second method refers to the time consumption needed to acquire a workable Raman signal intensity. Note that thin film absorber layers are characterized by a large absorption coefficient. The in depth method that we propose in this work combines several wavelengths with different focus depths. The use of longer wavelengths allows deeper focus on the sample without loss of Raman signal intensity. This is due to an inverse relationship between wavelength and absorption coefficient. Another feature refers to the possibility of using excitation wavelength with an energy close to the band gap of the material. This means that the measurement conditions are in a quasi-resonant mode

*Corresponding author.
**Present address: Uppsala University, Solid State Electronics, P.O. Box 534, SE-75121 Uppsala, Sweden
*Email addresses:* pafernandes@ua.pt (P. A. Fernandes), psalome@ua.pt (P.M.P. Salomé), antonio.cunha@ua.pt (A.F. da Cunha)

| CZTS [15] | | tetragonal-$Cu_2SnS_3$ [15] | | | cubic-$Cu_2SnS_3$ [15] | | | cubic-ZnS [15] | | |
|---|---|---|---|---|---|---|---|---|---|---|
| $2\theta$ (°) | h k l | $2\theta$ (°) | h k l | $\Delta$ (°) | $2\theta$ (°) | h k l | $\Delta$ (°) | $2\theta$ (°) | h k l | $\Delta$ (°) |
| 28.44 | 1 1 2 | 28.54 | 1 1 2 | 0.10 | 28.45 | 1 1 1 | 0.002 | 28.50 | 1 1 1 | 0.06 |
| 32.93 | 2 0 0 | 33.07 | 2 0 0 | 0.14 | 32.96 | 2 0 0 | 0.03 | 33.03 | 2 0 0 | 0.09 |
| 33.02 | 4 0 0 | - | - | - | - | - | - | - | - | - |
| 47.33 | 2 0 4 | 47.47 | 1 1 2 | 0.15 | 47.31 | 2 2 0 | 0.02 | 47.40 | 2 2 0 | 0.08 |
| 56.09 | 3 1 2 | 56.32 | 3 1 2 | 0.13 | 56.13 | 3 1 1 | 0.04 | 56.24 | 3 1 1 | 0.16 |
| 56.20 | 1 1 6 | - | - | - | - | - | - | - | - | - |
| 76.41 | 3 3 2 | 76.68 | 3 1 6 | 0.27 | 76.39 | 3 3 1 | 0.02 | 76.56 | 3 3 1 | 0.14 |

Table 1: Main XRD peaks and orientation planes for CZTS, tetragonal and cubic phases of CTS and cubic-ZnS. Estimation of the peak deviation, $\Delta$, of each phase in comparison to the CZTS peak.

which significantly increases the intensity of the Raman signal [9].

The first part of this work, section 2, compiles the information of CZTS and related chalcogenide phases XRD analysis. A brief description of the structural properties of this compounds is presented. The main part of this section is devoted to explaining the limitations of this technique in terms of phase identification.

A brief description of the details used to grow the various phases are presented in section 3. The experimental procedure described in the section is based in previously published work [2, 10–13], except for the growth of the cubic-ZnS phase.

The section 4.1 presents preliminary results of the characterization of a CZTS film based on structural and phase identification using the XRD and Electron Backscattered Diffraction (EBSD) techniques. The composition of the CZTS film is also analysed using energy dispersive spectroscopy (EDS) and inductively coupled plasma mass spectrometry (ICP-MS). In Section 4.2 it is presented the Raman scattering analysis' results for the various binary and ternary phases that may be present in a CZTS film. These results are very important for the ensuing discussion. In the last part, Section 4.3, a detailed study of the CZTS depth Raman scattering analysis employing several excitation wavelengths is shown. Additional information can be obtained when compared with the results obtained by XRD and EBSD in Section 4.1.

## 2. XRD analysis

CZTS crystallizes with the kesterite/stannite structure, I-4/I-42m space group which is of the adamantine family [14]. Its unit cell parameters are *a*: 5.435 Å and *c*: 10.843 Å [15]. Since it is a quaternary compound, it is possible that at the end of the growth process secondary and ternary phases may remain as well. The most likely to persist are $Cu_{2-x}S$, ZnS, $Sn_xS_y$, $MoS_2$ and different phases of $Cu_xSnS_{x+1}$ depending on the growth conditions.

$Cu_{2-x}S$ phases are easy to identify in XRD when in a phase mixture with CZTS because its diffraction peaks are clearly distinct from the CZTS ones. $Cu_{2-x}S$ phases can also be easily removed with a KCN treatment [11] and thus are not seen as a problem.

$Sn_xS_y$ phases can be SnS, $SnS_2$ and $Sn_2S_3$ [10], and are also easily identifiable by XRD. Our preliminary studies have shown that these phases are only present when the composition of the films is very Sn rich [10].

| Phase | Prec. order | $T_{sulf}$ (°C) | Pressure (mbar) |
|---|---|---|---|
| CZTS | SLG/Zn/Cu/Sn | 520 | 0.5 |
| tetrag.-$Cu_2SnS_3$ | SLG/Sn/Cu | 300 | 0.5 |
| cubic-$Cu_2SnS_3$ | SLG/Sn/Cu | 350 | 0.5 |
| Orth.-$Cu_3SnS_4$ | SLG/Sn/Cu | 520 | 0.5 |
| ZnS | SLG/Zn | 520 | 5.0 |
| $Sn_xS_y$ | SLG/Sn | 520 | 5.0 |

Table 2: Growth parameters for CZTS, CTS, ZnS and $Sn_xS_y$ phases.

Regarding ZnS, the identification of this phase using XRD is difficult if not impossible. The most probable ZnS phase to form is the cubic phase with a lattice parameter, *a*, of 5.410 Å. The amount of ZnS present in CZTS thin films is expected to be small and since there is only a small difference between the unit cell sizes, all of the XRD peaks of this structure are less than 0.2° apart from the CZTS ones as shown in Table 1.

Among the different $Cu_xSnS_{x+1}$ (CTS) phases, the ones that may be formed during the growth of CZTS are tetragonal-$Cu_2SnS_3$, cubic-$Cu_2SnS_3$ and orthorhombic-$Cu_3SnS_4$ [2, 12]. From these, only the orthorhombic-$Cu_3SnS_4$ is easy to identify using XRD. The cubic and the tetragonal have the same problem as ZnS, which is the unit cell sizes are quite similar to the CZTS ones. For the cubic phase, the *a* constant is 5.430 Å whereas for the tetragonal *a* has the value 5.413 Å with *c* taking the value of 10.824 Å [12]. The peak proximity for CZTS and CTS compounds are also presented in Table 1.

It is clear that considering the results shown in Table 1, the phase identification of samples constituted by a phase mixture can be a difficult task if only the XRD technique is used. The use of High Resolution XRD technique allied with numerical methods, such as Rietveld refinement, can help, but it will always depend on the quality of the sample, namely the crystallinity, compactness and strain characteristics.

## 3. Experimental Methods

### *3.1. Preparation of the films*

The method used for the growth of the CZTS, CTS, ZnS and $Sn_xS_y$ films consisted in the deposition of metallic precursor

| Sample/phase | Cu(%) | Zn(%) | Sn(%) | $\frac{[Cu]}{[Zn]+[Sn]}$ | $\frac{[Zn]}{[Sn]}$ | $\frac{[Cu]}{[Zn]}$ | $\frac{[Cu]}{[Sn]}$ |
|---|---|---|---|---|---|---|---|
| CZTS | 47.14±0.76 | 28.49 1.62 | 24.37±1.48 | 0.89±0.04 | 1.17±0.10 | 1.66±0.10 | 1.93±0.12 |
| tetra-CTS | 68.33±2.45 | - | 31.67±2.61 | - | - | - | 2.16±0.19 |
| cubic-CTS | 69.08±2.74 | - | 30.92±2.89 | - | - | - | 2.23±0.23 |
| orth-CTS | 74.61±2.83 | - | 25.39±2.11 | - | - | - | 2.94±0.27 |

Table 3: Atomic percentage and ratios for metallic elements for CZTS and CTS samples using EDS measurements.

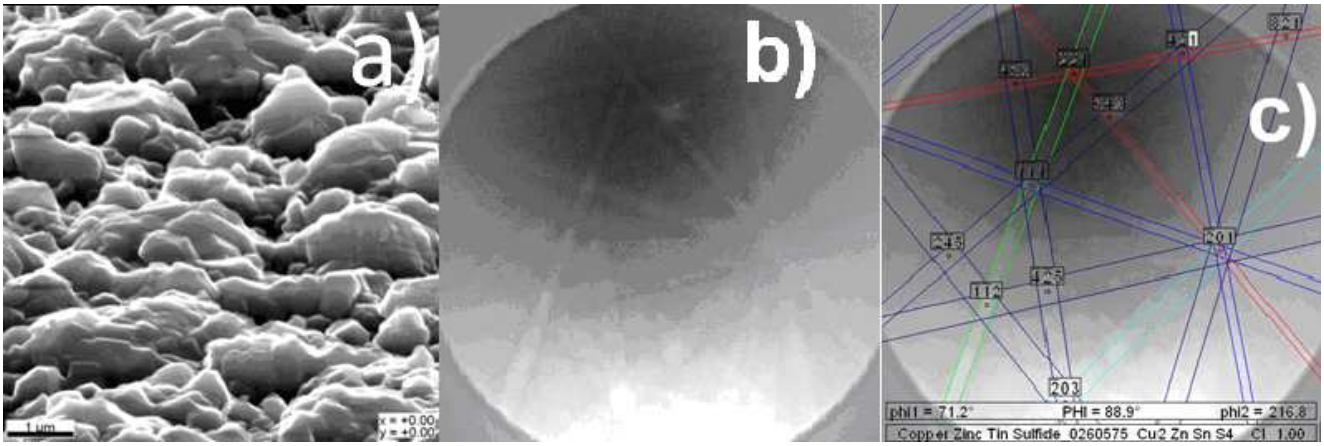


Figure 1: a) SEM micrograph of the CZTS surface, b). EBSD image and c). EBSD fitting confirming the presence of CZTS.

layers using dc-magnetron sputtering and a final annealing /sulphurization process [11–13].

The process starts with the substrate cleaning (3×3 $cm^2$ soda lime glass) which consist in successive ultrasound baths of acetone/ethanol/deionised water and its subsequent drying process with a $N_2$ flow. Next, the deposition of Mo back contact was performed by dc-magnetron sputtering from a Mo target with purity 3N as described by Salomé *et al.* [16]. The metallic precursors were deposited sequentially using dc-magnetron sputtering for the ternary and quaternary compounds. The deposition order used was Mo/Zn/Cu/Sn/ and /Sn/Cu/ for CZTS and CTS, respectively [11, 12]. For the growth of the binary sulphides only 1 deposition was necessary [13]. All precursor depositions were done under an Ar atmosphere, an operating pressure of $2\times10^{-3}$ mbar and power densities of 0.16 $Wcm^{-2}$, 0.36 $W/cm^{-2}$ and 0.11 $Wcm^{-2}$ for Cu, Zn and Sn, respectively. The distance between the target and the substrate was set to 8 cm. The purity of the targets was 5N for Cu and 4N for Zn and Sn. In situ thickness' monitoring was performed with a quartz crystal monitor. No Mo layer was used in the growth of the binary and ternary compounds.

The crystal formation was performed in a tubular furnace in a nitrogen plus sulphur vapour atmosphere at a constant working pressure and a $N_2$ flow rate of 40 ml/min. The sulphur pellets with purity 5N, were evaporated at 130 °C in a temperature controlled quartz tube source. The furnace temperature increased at 10 °C/min. The maximum temperature was kept constant during 10 min and then the system was set to cool down naturally. Some growth parameters are summarized in Table 2.

Unwanted phases, such as $Cu_{2-x}S$, that were formed during the CZTS and CTS crystallization process were eliminated using a KCN chemical treatment [11]. The samples were, sequentially, submitted to the KCN solution at 10 % w/w, a solution of ethanol/deionised water at 50 % vol/vol and finally deionised water. Each step had duration of 2 min. Finally, all samples were dried with a $N_2$ gas flux.

### *3.2. Sample characterization*

The composition of the films was analysed by EDS using a S4100 Hitachi with a Rontec EDS system and confirmed with an ICP-MS Thermo X Series. XRD was done with a PHILIPS PW 3710 with a $CuK_\alpha$ line of 1.5406 Å . SEM and EBSD measurements were done with a FEI Quanta 400 FEG ESEM device equipped with an EDAX Genesis X4M system. Raman scattering spectroscopy was done using a Jobin Yvon T64000 Raman scattering system with an Olympus microscope equipped with a 100X magnification lens and in the backscattering configuration. All the Raman scattering measurements were performed using an excitation wavelength of 488 nm, with the exception of the measurements presented in the depth study, Section 4.3, where the excitation wavelengths used were 488 nm, 514 nm, 633 nm and 785 nm.

XRD analysis was also used to confirm that the CTS samples were single phase. Detailed results were presented by Fernandes *et al.* [2, 12].

The absorption coefficient was estimated from the transmittance and reflectance data, measured with a Shimadzu UV3600 spectrophotometer, using the following equation:

$$\alpha = -\frac{1}{h}\frac{-(1-R)^2 + \sqrt{(1-R)^4 + 4T^2R^2}}{2TR^2} \quad (1)$$

where $\alpha$ is the absorption coefficient, $h$ the thickness of the sample, $R$ the reflectance and $T$ the transmittance.

## 4. Results and discussion

### *4.1. Preliminary CZTS film analysis*

The sample's composition was analysed by EDS and confirmed using ICP-MS for metallic elements (not shown).. The atomic percentage, atomic ratios and experimental uncertainties, measured by EDS, for the CZTS and CTS phases, are shown in Table 3. These compositions are close to the ones reported by Katagiri *et al.* [4] for their CZTS solar cell with best efficiency. In Table 3 no sulphur content is presented for these samples, but for samples grown directly on SLG using the same sulphurization conditions, EDS measurements presented concentrations between 48.5% and 51.3% for all the studied samples, except for the sample where $Sn_xS_y$ phases were grown. In this case the sulphur concentration was close to 59%. This means that the sulphurization of the precursors was completed. Neither EDS nor ICP-MS are capable of measuring the quantity of sulphur present in the sample when Mo is present. EDS cannot resolve sulphur from Mo due to the overlapping energy peaks, namely Mo $L_\alpha$ and S $K_\alpha$. A method to overcome this problem is to grow the compound directly over the glass substrate to avoid the presence of Mo. This approach does not allow the solar cell conclusion (no back contact is deposited) and the absorber layer properties could be altered due to the fact that it is grown on a different substrate. Wavelength Dispersive Spectroscopy (WDS) which present a higher resolution than EDS can perform the deconvolution of the energy peaks of sulphur and Mo elements. ICP-MS present some limitations to the quantification of the sulphur mainly due to ionization and oxygen interference problems. This technique is more suitable to quantify the stacked metallic precursors.

The SEM micrograph of the CZTS sample surface, in Figure 1-a), shows a rough film with some voids. EBSD was performed on this film. Several random points were analyzed using the EBSD method and all the results showed single phase CZTS. The Figure 1-b) presents the EBSD image and its fitting is shown in Figure 1-c). This analysis only showed the presence of CZTS with the kesterite structure.

The EBDS structural analysis was confirmed with XRD and the results are shown in Figure 2. Besides the Mo, only CZTS with the kesterite structure was found with its diffractions peaks identified.

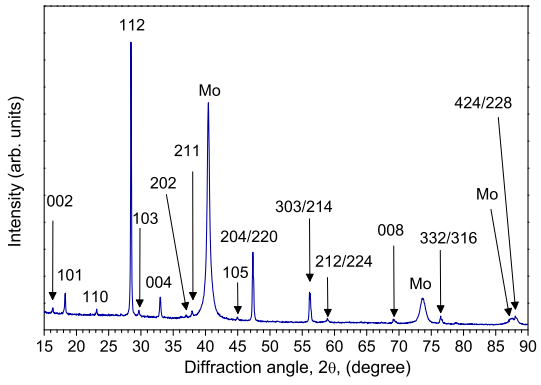


Figure 2: XRD diffraction pattern of a CZTS film deposited on Mo coated soda lime glass.

| Phase | Raman scattering peak ($cm^{-1}$) | References |
|---|---|---|
| CZTS | 289, 339, 350, 370 | [10, 17] |
| tetrag.-CTS | 297, 337, 352 | [2, 12] |
| cubic-CTS | 267, 303, 356 | [2, 12] |
| orth.-CTS | 318 | [2, 12] |
| cubic-ZnS | 275, 352 | [20] |
| SnS | 160, 190, 219 | [21] |
| $SnS_2$ | 314 | [21] |
| $Sn_2S_3$ | 32, 60, 307 | [21] |
| $Cu_{2-x}S$ | 475 | [22] |
| $MoS_2$ | 288, 384, 410 | [18, 19] |

Table 4: Summary of the Raman peaks location of the CZTS, ternary and binary phases.

### *4.2. Raman spectra of CZTS and other binary and ternary phases in the CZTS film*

Before analysing CZTS films possibly containing several unwanted phases it is crucial to know at what energies occur the Raman peaks for the different phases. In Figure 3, the Raman scattering spectra of several phases, most likely to appear in CZTS films, are presented with their most prominent peaks identified. CZTS is known to have the following strong peaks: 288-289 $cm^{-1}$ and 338-239 $cm^{-1}$ [10, 17] as shown in Figure 3-a). There is a broad peak between 368-373 $cm^{-1}$ and a shoulder of the main peak at 351 $cm^{-1}$ [10, 17]. The latter two peaks appear only in certain conditions which are still not clearly identified. Hexagonal $MoS_2$, Figure 3-b), has three peaks, 288 $cm^{-1}$, 384 $cm^{-1}$ and 410 $cm^{-1}$, these peaks are according to Sandoval *et al.* [18] and Fernandes *et al.* [19]. ZnS can be identified by the strong peak at 352 $cm^{-1}$, Figure 3-c), and a weaker one at 275 $cm^{-1}$ [20]. For the tetragonal $Cu_2SnS_3$, Figure 3-d), there is a big shoulder in the region between 280 $cm^{-1}$ and 290 $cm^{-1}$ and it appears that the peak maximum is at 297 $cm^{-1}$. This phase presents two other peaks at 337 $cm^{-1}$ and 352 $cm^{-1}$ [2, 12]. However, previous studies show that this phase is not preferential at the high growth temperatures of CZTS [2] and therefore is not likely to remain after the growth of CZTS process is concluded. Cubic $Cu_2SnS_3$, Figure 3-e), has three visible peaks at 267 $cm^{-1}$, 303 $cm^{-1}$ and 356 $cm^{-1}$ [2, 12]. Orthorhombic $Cu_3SnS_4$, Figure 3-f), has only one peak visible at 318 $cm^{-1}$ [2, 12]. SnS has three peaks at 160 $cm^{-1}$, 190 $cm^{-1}$ and 219 $cm^{-1}$ [21], Figure 3-g), and $SnS_2$, Figure 3-h), has one strong peak at 314 $cm^{-1}$ [21], if the crystal quality is good enough, other weak peaks may appear at lower energies. In the course of this work we were not able to grow single-phase $Sn_2S_3$ thin films, but from the literature it is known that this compound has peaks at 52 $cm^{-1}$, 60 $cm^{-1}$ and 307 $cm^{-1}$ [21]. $Cu_{2-x}S$ compounds have their strongest peak at 475 $cm^{-1}$ [22] as shown in Figure 3-i).

Table 4 shows the list of Raman peaks' position and references of the chalcogenide compounds used to identify the phases present.

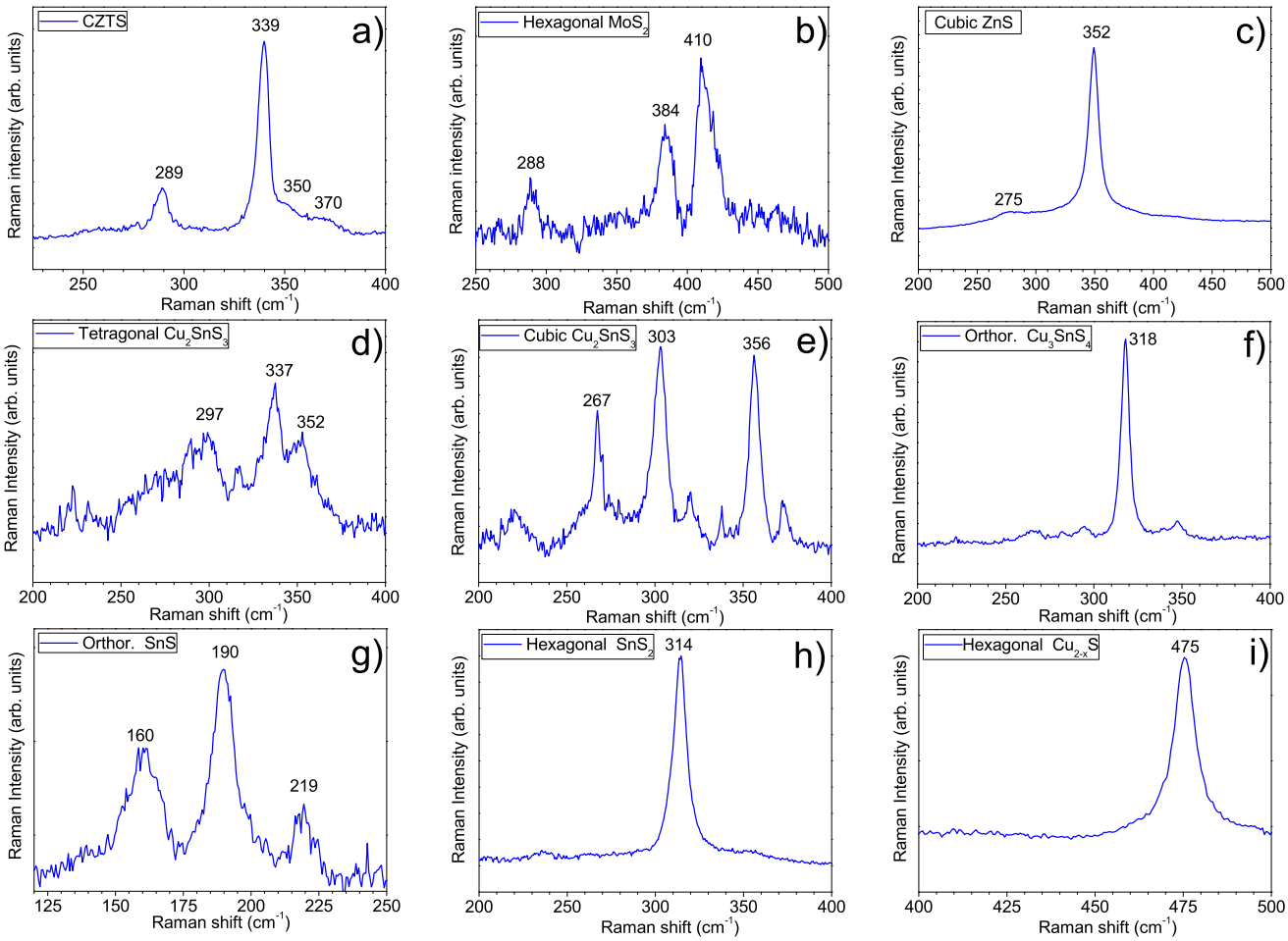


Figure 3: Raman scattering spectra for different single phase reference compounds. The excitation laser wavelength was 488 nm.

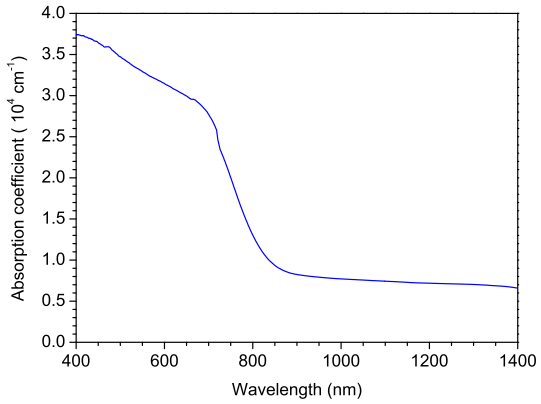


Figure 4: Absorption coefficient as function of wavelength for the CZTS thin film under study.

| Wavelength (nm) | Absorption ($cm^{-1}$) | Analysis' effective depth (nm) |
|---|---|---|
| 488 | $3.5\times10^4$ | 140 |
| 514 | $3.4\times10^4$ | 150 |
| 633 | $3.0\times10^4$ | 170 |
| 785 | $1.5\times10^4$ | 400 |

Table 5: Raman scattering analysis' effective depths for different excitation wavelengths.

### *4.3. CZTS films' depth Raman scattering analysis*

Now that the phases, most likely to appear when growing CZTS films, were individually studied, it is then possible to make a more detailed analysis of multi-phase thin films. Before that, let us consider the absorption coefficient behaviour as a function of the wavelength for CZTS, as shown in Figure 4. This Figure presents the behaviour of a direct band gap semiconductor with a maximum value of absorption coefficient just below $4\times10^4$ $cm^{-1}$. For a semiconductor, the light penetration depth, $d$, is roughly given by $d = 1/\alpha$, where $\alpha$ is the absorption coefficient. In the case of Raman scattering analysis using the back scattering configuration, one must consider that the light must return and therefore the equation is then $d \approx 1/(2\alpha)$. Using this equation and knowing $\alpha$, one can roughly estimate the depth to which most of the Raman scattering analysis extends when using different excitation laser wavelengths. Using the data from the curve shown in Figure 4, it is possible to estimate the effective penetration depth shown in Table 5. It can be seen that for a variation of the wavelength between 488 and 633 nm, there is practically no difference in the effective penetration depth, ranging from 140 to 170 nm, but if a wavelength of 785 nm is used it is possible to go down to 400 nm.

Figure 5 presents the Raman spectra of the CZTS thin film using different excitation laser wavelengths. The main peak of CZTS, P1, is located at 338-339 $cm^{-1}$, it has been associated to the vibration of sulphur atoms [23] and is the strongest peak at all excitation wavelengths. This is strong evidence that CZTS with the kesterite/stannite structure is the dominant phase present. The second peak of CZTS, P2, at 287-288 $cm^{-1}$, is also present for all excitation wavelengths. The third peak of CZTS, P3, located at 367-368 $cm^{-1}$, is much more intense at the ex-

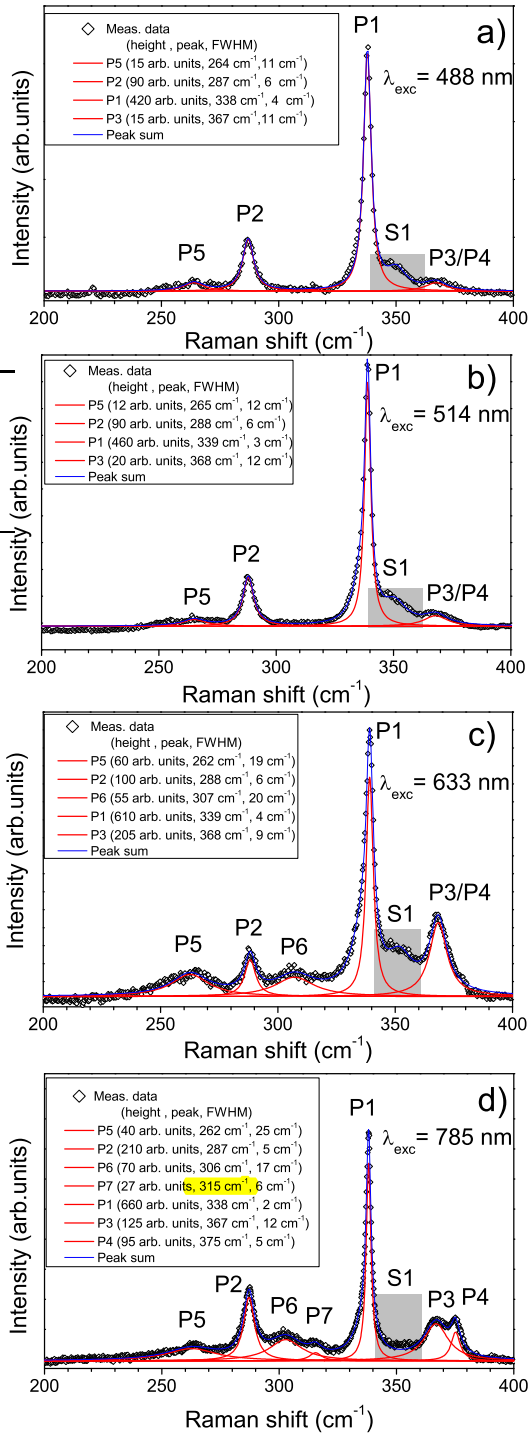


Figure 5: Raman scattering analysis, of the CZTS films, using different excitation laser wavelengths.

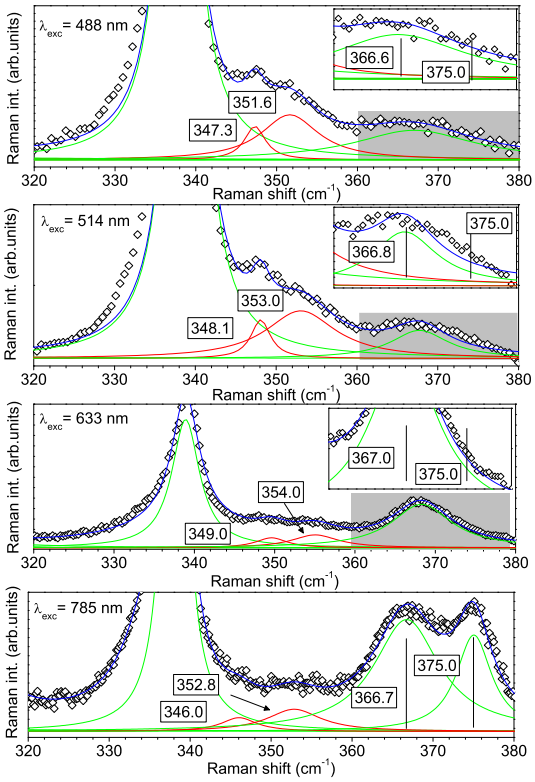


Figure 6: Details of the CZTS Raman scattering spectra showing the shoulder S1, using different excitation laser wavelengths. Inset graphs show the Raman spectra for wavenumbers between 360 $cm^{-1}$ and 380 $cm^{-1}$

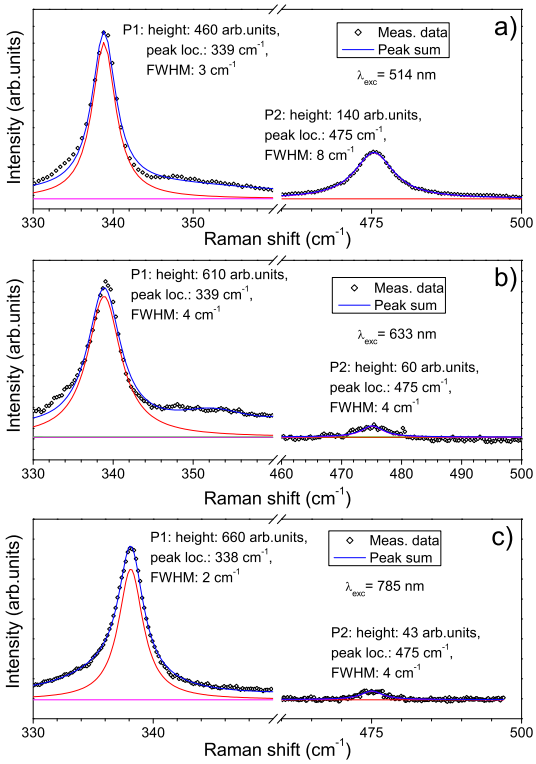


Figure 7: Analysis of the CZTS Raman peak, 338 $cm^{-1}$ and the $Cu_{2-x}S$ Raman peak at 475 $cm^{-1}$ using different excitation laser wavelengths.

citation wavelengths of 633 nm and 785 nm. This behaviour is more evident for the peak P4 at 375 $cm^{-1}$ which presents a higher intensity at the wavelength of 785 nm. A shoulder of the main peak, S1, at 350 $cm^{-1}$, is present at all excitation wavelengths. The spectra presented in figure 5 also show a peak, P5 located close to 263 $cm^{-1}$. A more detailed analysis of the shoulder S1 and the peaks P3 and P4 is shown in figure 6.

A special attention is taken for the S1 shoulder analysis, due to the fact that cubic-ZnS has a peak close to 350 $cm^{-1}$. The deconvolution of this shoulder is presented in Figure 6. These results show 2 peaks located close to 348 and to 352-353 $cm^{-1}$. Comparing this data with the results shown in figure 3-c) the higher energy peak can be assigned to the cubic-ZnS vibration mode. On the other hand the Raman mode at 348 $cm^{-1}$ is attributed to CZTS. Note that no other phase with Raman modes close to these values are detected in these spectra. The closer one is the cubic-CTS with a mode close to 356 $cm^{-1}$. The Raman spectrum for the case of the excitation wavelength of 633 nm seems to present this CZTS mode at 354 $cm^{-1}$ but a closer look to these values show that all values are shifted up approximately 1 $cm^{-1}$ due to an inadequate calibration of the Raman system. The detection of peaks 348 $cm^{-1}$ and 353 $cm^{-1}$ allows the detection of the cubic-ZnS in a solid mixture of the CZTS with this phase. Other results shown in figure 6 refer to peaks P4 at 375 $cm^{-1}$. For the excitation wavelength 488 nm, 514 nm and 633 nm and for Raman wavenumbers higher than 370 $cm^{-1}$ the peak sum (in blue) presents lower values than the measured ones. These results are presented in more detail in the inset graphs of figure 6. These differences mean that the fittings were not good enough and it is likely that the 375 $cm^{-1}$ modes are missing in these analyses. Unfortunately, this task has not been realized due to difficulties associated with the fitting of modes whose intensities are so low. Despite that, it seems that the peak P4 at 375 $cm^{-1}$ attributed to the CZTS phase became more active for the wavelength 785 nm.

In general the Raman scattering spectra for the excitation lines of 488 nm and 514 nm are very similar; this is in accordance with the similar effective penetration depth values estimated before, 140 nm and 150 nm, respectively. However for the excitation wavelength of 633 nm, for which the analysis' effective depth of 170 nm was estimated, there are already some identifiable differences. A peak at 307 $cm^{-1}$ is found which is attributed to the binary chalcogenide $Sn_2S_3$. For the excitation wavelength of 785 nm, an additional peak at 315 $cm^{-1}$ is found. This peak is assigned to the $SnS_2$ compound, which has a peak at 314 $cm^{-1}$.

It is likely that below 170 nm $Sn_2S_3$ is present in small traces since the peaks found are small when compared with the CZTS peaks. For a deeper region, below 400 nm, the small peak at 315 $cm^{-1}$ points to the presence of $SnS_2$ phase, but as for $Sn_2S_3$, due to its low intensity only a residual quantity is expected.

The Raman scattering data, in Figure 7, allow us, also, to evaluate the depth to which the $Cu_{2-x}S$ phases extend. That is done by studying the evolution of the intensity ratios between the main CZTS peak, at 338-339 $cm^{-1}$ and that of $Cu_{2-x}S$, at

| Excitation Wavelengths (nm) | I338/I475 |
|---|---|
| 514 | 3.3 |
| 633 | 10.2 |
| 785 | 15.3 |

Table 6: Intensity ratio of the 338 $cm^{-1}$ CZTS Raman scattering peak and of the 475 $cm^{-1}$ $Cu_{2-x}S$ one.

475 $cm^{-1}$. This was done for the excitation wavelengths of 514 nm, 633 nm and 785 nm as is shown in Table 6. We conclude that the $Cu_{2-x}S$ phases are mostly located at the surface of the sample since the I338/I475 value increases rapidly with the excitation wavelength, which means that for increased depth there is more signal coming from the CZTS than from $Cu_{2-x}S$. After this analysis the films were subjected to a KCN treatment and the Raman scattering $Cu_{2-x}S$ peaks disappeared for all the excitation wavelengths, which may confirm that the $Cu_{2-x}S$ compounds were distributed at the surface.

The XRD results, presented in Figure 2 showing single phase CZTS films, seem to be in disagreement with the Raman scattering results shown in Figure 5, namely for the $Sn_2S_3$ and $SnS_2$ phases, which can be resolved by both XRD and Raman scattering. Cubic ZnS phase is also detected in the films as the deconvolutions showed. In $\mu$-Raman scattering technique, unlike XRD, the interaction volume is more confined, allowing a more localized or detailed analysis of the sample. This feature helps to detect residual phases that could be present. So residual phases like the ones we are describing can be hidden in noise level, because these quantities are below the detection capabilities of XRD

## 5. Conclusion

The main result of this work was the demonstration that Raman scattering as complementary technique to XRD in the structural analysis of polycrystalline CZTS films is a very valuable tool, allowing for an increased ability in resolving the different undesired phases that may be present. It was also demonstrated that with this approach it is possible to locate the various phases tri-dimensionally.

We have shown that our CZTS films prepared with chemical composition, verified by complementary techniques such as EDS and ICP-MS, identical to the one reported by Katagiri *et al.* [4] for their record efficiency CZTS solar cells, still presented undesired phases such as $Sn_2S_3$. The results also hint for the presence of $SnS_2$ in residual quantities due to the weak relative intensity of the corresponding Raman scattering peaks. These findings could not be confirmed by XRD and EBSD analysis since they pointed to a single phase CZTS film. Our analysis confirms that our samples are composed mainly by the CZTS phase, and such statement cannot be done using only XRD analysis. Using Raman scattering techniques we also detected the presence of cubic-ZnS.

Finally, this work shows that preparing single phase CZTS film is not a simple task and thus a depth study of the influence of the unwanted phases on solar cell performance is required to go beyond the current best results.

## 6. Acknowledgements

P. A. Fernandes thanks the financial support of the Fundação para a Ciência e Tecnologia (FCT), Portugal, through a PhD grant number SFRH/BD/49220/2008. FCT is also acknowledged for the financial support of the national electronic microscopy network, whose services we have used, through the grant REDE/1509.

## References

[1] H. Katagiri, M. Nishimura, T. Onozawa, S. Maruyama, M. Fujita, T. Sega and T. Watanabe, Masato Fujita, Toshiyuki Sega and T. Watanabe, PCC-Nagaoka '97, IEEE, (1997), 1003.
[2] P. A. Fernandes, P. M. P. Salomé and A. F. da Cunha, Phys. Status Solidi C, 7, No. 3-4, (2010), 901.
[3] Zentrum für Sonnenenergie und Wasserstoff - Forschung Baden-Wurttemberg, "ZSW produces a thin-film solar cell with 20.3 percent efficiency", Press release 08/2010, (2010), Stuttgart, Germany.
[4] H. Katagiri, K. Jimbo, S. Yamada, T. Kamimura, W. S. Maw, T. Fukano, T. Ito, and T. Motohiro, Appl. Phys. Express, 1, (2008), 041201.
[5] R. Klenk, J. Klaer, R. Scheer, M.Ch. Lux-Steiner, I. Luck, N. Meyer and U. Rühle, Thin Solid Films, 480, (2005) 509.
[6] R. Takei, H.Tanino, S.Chichibu and H.Nakanishi, J. Appl. Phys., 79, (1996), 2793.
[7] L. Calvo-Barrio, A. Pérez-Rodríguez, J. Alvarez-García, A. Romano-Rodríguez, B. Barcones, J. R. Morante, K. Siemer, I. Luck, R. Klenk and R. Scheer, Vacuum, 63, 1-2, (2001), pp 315-321.
[8] J. Álvarez-García, A. Pérez-Rodríguez, A. Romano-Rodríguez, L. Calvo-Barrio, B. Barcones, J. R. Morante, K. Siemer, I. Luck and R. Klenk, Thin Solid Films, 387, 1-2, 29, (2001), 219.
[9] . V. Izquierdo-Roca, A.Shavel, E.Saucedo, S.Jaime-Ferrer, J. Álvarez-García, A.Cabot, A. Pérez-Rodríguez, V.Bermudez, J.R.Morante, Sol. Energy Mater. Sol. Cells, (2010), doi:10.1016/j.solmat.2010.11.014
[10] P.A. Fernandes, P.M.P. Salomé and A.F. da Cunha, Thin Solid Films, 517, (2009), 2519.
[11] P. A. Fernandes, P. M. P. Salomé and A. F. da Cunha, Semicond. Sci. Technol. 24, (2009), 105013.
[12] P. A. Fernandes, P. M. P. Salomé and A. F. da Cunha, J. Phy. D. Appl. Phys., 43, (2010), 215403.
[13] J. Malaquias; P. A. Fernandes; P.M.P. Salomé; A.F. da Cunha, accepted for publication,2011, Thin Solid Films.
[14] S. Schorr, Thin Solid Films, 515, (2007), 5985.
[15] International Centre for Diffraction Data reference 04-005-0388 (CZTS), 01-089-4714 (tetragonal-$Cu_2SnS_3$), 01-089-2877 (cubic-$Cu_2SnS_3$), 04-006-0807 (cubic-ZnS).
[16] P. M. P. Salomé, J. Malaquias, P. A. Fernandes and A. F. da Cunha, J. Phys. D: Appl. Phys. 43 (2010) 345501.
[17] M. Altosaar, J. Raudoja, K. Timmo, M. Danilson, M. Grossberg, J. Krustok and E. Mellikov, Phys. Status Sol(a). 205, (2008), 167.
[18] S. Jiménez Sandoval, D. Yang, R. F. Frindt and J. C. Irwin, Physical Review B, 44, 8, (1991), 3955.
[19] P. A. Fernandes; P.M.P. Salomé; A.F. da Cunha; Björn-Arvid Schubert, Thin Solid Films, doi: 10.1016/j.tsf.2010.12.035.
[20] W. G. Nilsen, Phys Rev, 182 (1969) 838.
[21] Louise S. Price, Ivan P. Parkin, Amanda M. E. Hardy and Robin J. H. Clark, Chem. Mater., 11 ,(1999), 1792.
[22] Carolyn G. Munce, Gretel K. Parker, Stephen A. Holt , Gregory A. Hope, Colloids and Surfaces A : Physicochem. Eng. Aspects, 295, (2007) 152.
[23] M. Himmrich and H. Haeuseler, Spectrochemica Acta, 47A, 7, (1991) 933.

***Research Highlights**

***Highlights***

- Description of the characterization problems using XRD analysis in $Cu_2ZnSnS_4$ thin films;
- Raman in depth analysis using different laser excitation wavelengths;
- Cubic-ZnS phase detection in a $Cu_2ZnSnS_4$ solid mixture by Raman scattering.